Rituximab and obinutuzumab differentially hijack the B-cell receptor and NOTCH1 signaling pathways

EDELMANN, Jennifer, DOKAL, Arran D., VILVENTHRARAJA, Emma, HOLZMANN, Karlheinz, BRITTON, David, KLYMENKO, Tetyana, DÖHNER, Hartmut, CRAGG, Mark, BRAUN, Andrejs, CUTILLAS, Pedro and GRIBBEN, John G.

iScience

CellPress
OPEN ACCESS

Article

Rituximab and obinutuzumab differentially hijack the B cell receptor and NOTCH1 signaling pathways

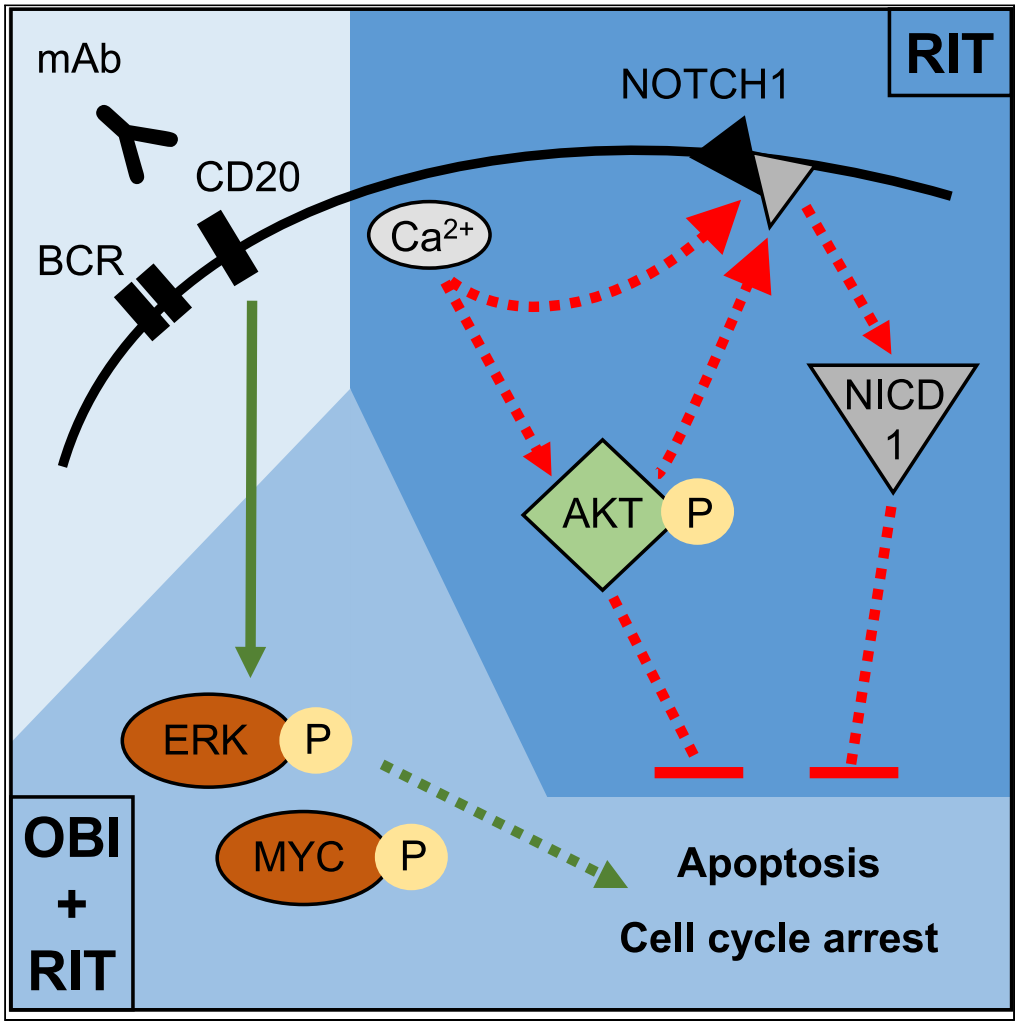

Jennifer Edelmann, Arran D. Dokal, Emma Vilventhraraja, ..., Andrejs Braun, Pedro Cutillas, John G. Gribben

jennifer.edelmann@uni-ulm.de

HIGHLIGHTS

Rituximab and obinutuzumab induce strong ERK and MYC activation

Obinutuzumab supports apoptosis induction by aberrant SYK phosphorylation

Rituximab elicits stronger anti-apoptotic signals by activating AKT

Rituximab elicits stronger pro-survival signals by enhancing NOTCH1 signaling

Edelmann et al., iScience *24*, 102089
February 19, 2021
https://doi.org/10.1016/j.isci.2021.102089

iScience

CellPress
OPEN ACCESS

Article

Rituximab and obinutuzumab differentially hijack the B cell receptor and NOTCH1 signaling pathways

Jennifer Edelmann,[1,2,7,*] Arran D. Dokal,[1,3] Emma Vilventhraraja,[1] Karlheinz Holzmann,[4] David Britton,[1,3] Tetyana Klymenko,[1,5] Hartmut Döhner,[2] Mark Cragg,[6] Andrejs Braun,[1] Pedro Cutillas,[1,3] and John G. Gribben[1]

SUMMARY

The anti-CD20 monoclonal antibodies rituximab and obinutuzumab differ in their mechanisms of action, with obinutuzumab evoking greater direct B cell death. To characterize the signaling processes responsible for improved B cell killing by obinutuzumab, we undertook a phosphoproteomics approach and demonstrate that rituximab and obinutuzumab differentially activate pathways downstream of the B cell receptor. Although both antibodies induce strong ERK and MYC activation sufficient to promote cell-cycle arrest and B cell death, obinutuzumab exceeds rituximab in supporting apoptosis induction by means of aberrant SYK phosphorylation. In contrast, rituximab elicits stronger anti-apoptotic signals by activating AKT, by impairing pro-apoptotic BAD, and by releasing membrane-bound NOTCH1 to upregulate pro-survival target genes. As a consequence, rituximab appears to reinforce BCL2-mediated apoptosis resistance. The unexpected complexity and differences by which rituximab and obinutuzumab interfere with signaling pathways essential for lymphoma pathogenesis and treatment provide important impetus to optimize and personalize the application of different anti-CD20 treatments.

INTRODUCTION

Combination of the anti-CD20 monoclonal antibody rituximab with chemotherapy has significantly improved outcomes for patients with CD20$^+$ B cell lymphoma (Marshall et al., 2017). Despite this success, the mechanisms of action of rituximab remain incompletely understood, largely because they are manifold and encompass low levels of direct B cell killing next to immune-mediated effects (Marshall et al., 2017). The latter are mainly mediated by complement recruitment, but they also comprise antibody-dependent cellular cytotoxicity and phagocytosis (Marshall et al., 2017; Rouge et al., 2020). The clinical success of rituximab has fostered the development of novel anti-CD20 antibodies such as obinutuzumab with stronger capacity for direct B cell killing and a glycoengineered Fc-fragment for improved effector cell recruitment. Higher efficiency in the induction of direct B cell death was achieved by introducing a sequence alteration into the elbow-hinge region of the monoclonal antibody, rendering it more Type II, and so less able to cluster CD20 in the membrane, reducing complement-dependent cytotoxicity when compared with rituximab and other Type I monoclonal antibodies (Mossner et al., 2010). The molecular effects that this alteration has on B cell signaling are relatively undocumented. A non-apoptotic lysosomal form of cell death has been shown for obinutuzumab (Alduaij et al., 2011), whereas the limited degree of rituximab-induced cell death has been associated with apoptosis following increased B cell receptor (BCR) signaling (Walshe et al., 2008; Franke et al., 2011; Pavlasova et al., 2018).

Phase III clinical trials comparing rituximab and obinutuzumab head-to-head demonstrated superiority of obinutuzumab over rituximab in the treatment of chronic lymphocytic leukemia (CLL; CLL11 trial, ClinicalTrials.gov ID: NCT01010061) and follicular lymphoma (GALLIUM trial, ClinicalTrials.gov ID: NCT01332968) with regard to minimal residual disease negativity, progression-free survival (PFS), and in the case of CLL, overall survival (Goede et al., 2014, 2015; Marcus et al., 2017). However, in first-line treatment of diffuse large B cell lymphoma (DLBCL; GOYA trial; ClinicalTrials.gov ID: NCT01287741), obinutuzumab failed to show benefit over rituximab (Vitolo et al., 2017). The reasons for non-superiority of obinutuzumab in DLBCL treatment remain unresolved, partly due to a limited understanding of biomarkers predicting response to rituximab or obinutuzumab.

[1]Centre for Haemato-Oncology, Barts Cancer Institute, Queen Mary University of London, Charterhouse Square, London, EC1M 6BQ, UK

[2]Department of Internal Medicine III, Ulm University, Albert-Einstein-Allee 23, 89081 Ulm, Germany

[3]Kinomica Limited, Biohub Alderley Park, Alderley Edge, Macclesfield, Cheshire, SK10 4TG, UK

[4]Center for Clinical Research, Genomics Core Facility, Ulm University, Helmholtzstr. 8/1, 89081 Ulm, Germany

[5]Sheffield Hallam University, City Campus, Howard Street, Sheffield, S1 1WB, UK

[6]Antibody and Vaccine Group, Centre for Cancer Immunology, University of Southampton Faculty of Medicine, Tremona Road, Southampton, SO16 6YD, UK

[7]Lead contact

*Correspondence: jennifer.edelmann@uni-ulm.de

https://doi.org/10.1016/j.isci.2021.102089

One biomarker identified to predict decreased benefit from the addition of rituximab to fludarabine and cyclophosphamide in CLL treatment is the presence of *NOTCH1* mutation (Stilgenbauer et al., 2014). In contrast, obinutuzumab maintains beneficial effects in this CLL subgroup (Estenfelder et al., 2016). How the membrane-bound transcription factor NOTCH1 can interfere with rituximab-based chemoimmunotherapy is also unknown. NOTCH1 releases its intracellular domain (NICD1) after two cleavage steps executed by the disintegrin and metalloproteinases ADAM10 or ADAM17 and by the γ-secretase complex to up-regulate genes involved in B cell survival and resistance to apoptosis, proliferation, and differentiation (Borggrefe and Oswald, 2009; Fabbri et al., 2017; Santos et al., 2007). In B cell malignancies, most *NOTCH1* mutations result in a disruption of the PEST domain responsible for NICD1 inactivation and degradation (Fabbri et al., 2011; Weng et al., 2004; Stilgenbauer et al., 2014).

To characterize B-cell-intrinsic signaling events following rituximab and obinutuzumab treatment, we applied liquid chromatography-tandem mass spectrometry (LC-MS/MS)-based phosphoproteomics. We thereby uncovered an activation of pathways downstream of the BCR by rituximab as well as obinutuzumab treatment, identified differences between the two monoclonal antibodies, and discovered links between anti-CD20 treatment and NOTCH1 arising from an activation of the BCR signaling cascade.

RESULTS

Activation of BCR signaling

First, to validate a functionally relevant increase in BCR signaling by rituximab treatment, we measured *CCL4* and *CCL3* expression as established surrogates for BCR activation (Takahashi et al., 2015). Transcription of both genes was up-regulated following rituximab treatment ($p < 0.0001$). An increase in *CCL4* and *CCL3* expression was also observed after treating with rituximab $F(ab')_2$ fragments ($p < 0.001$), but not trastuzumab (Figure 1) demonstrating that the induction of BCR signaling was specific for CD20 binding and not engagement of the inhibitory FcγRIIB. R406 treatment to inhibit the spleen tyrosine kinase (SYK) reduced basal *CCL4* and *CCL3* expression levels ($p < 0.01$), diminished the increase in *CCL3* expression after rituximab treatment (mean fold changes 20.2 versus 3.8; $p < 0.001$), and completely abrogated *CCL4* up-regulation by rituximab (Figure 1), positioning signal generation by rituximab toward the proximal BCR signaling cascade. Increased BCR signaling as inferred by *CCL4* expression was also observed in MEC1 as well as in primary CLL cells after rituximab treatment (Figure S1).

To refine our understanding of rituximab-induced signaling events within the BCR signaling cascade and compare them with signals generated by obinutuzumab treatment, we used LC-MS/MS-based phosphoproteomics to analyze SU-DHL4 lymphoma cells after treating with rituximab or obinutuzumab for 1 or 24 h. Considering the two time points in both treatment arms relative to untreated control samples, we identified 41 protein kinases after rituximab and 40 protein kinases after obinutuzumab treatment with significantly altered activity as inferred by KSEA. Thirty-two of these kinases were affected by both rituximab and obinutuzumab, suggesting a high concordance between the signaling pathways modified by both antibodies (Figure 2). Pathway enrichment analyses of the affected kinases revealed activation of pathways belonging to the BCR signaling cascade and down-regulation of cell cycle progression subsequent to both antibody treatments (Table S1).

Excessively strong signals from the BCR lead to autoimmune checkpoint activation, cell-cycle arrest, and B cell apoptosis as a physiologic mechanism to negatively select B cells with a specificity for autoantigens (Muschen, 2018). To explore the hypothesis that rituximab and obinutuzumab hijack this mechanism to elicit direct B cell killing, we next analyzed ERK, SYK, and the PI3K in more detail, as strong activation of these three kinases has been shown to drive B cell selection (Muschen, 2018).

Differences between rituximab and obinutuzumab

The kinase with the strongest increase in activity at the 1 h time point after antibody treatment was identified as MEK, responsible for ERK activation (Figure 2). Consistently, ERK1 Thr^{202}/Tyr^{204} and ERK2 Thr^{185}/Tyr^{187} in the kinase activation loops had highly increased phosphorylation levels at this time point (4-fold and >10-fold increase, respectively; Figure 3A). The 24 h time point revealed lasting activity in the MEK-ERK signaling axis after rituximab treatment, whereas this longevity was not observed for obinutuzumab. The ERK target site MYC Ser^{62} had a 2-fold increase in phosphorylation at the 24 h time point uncovering activation of the MYC transcription factor. However, at the same time point, we also observed increased levels of Thr^{58}/Ser^{62} doubly phosphorylated MYC (4- to 5-fold) representing an already de-activated form of the

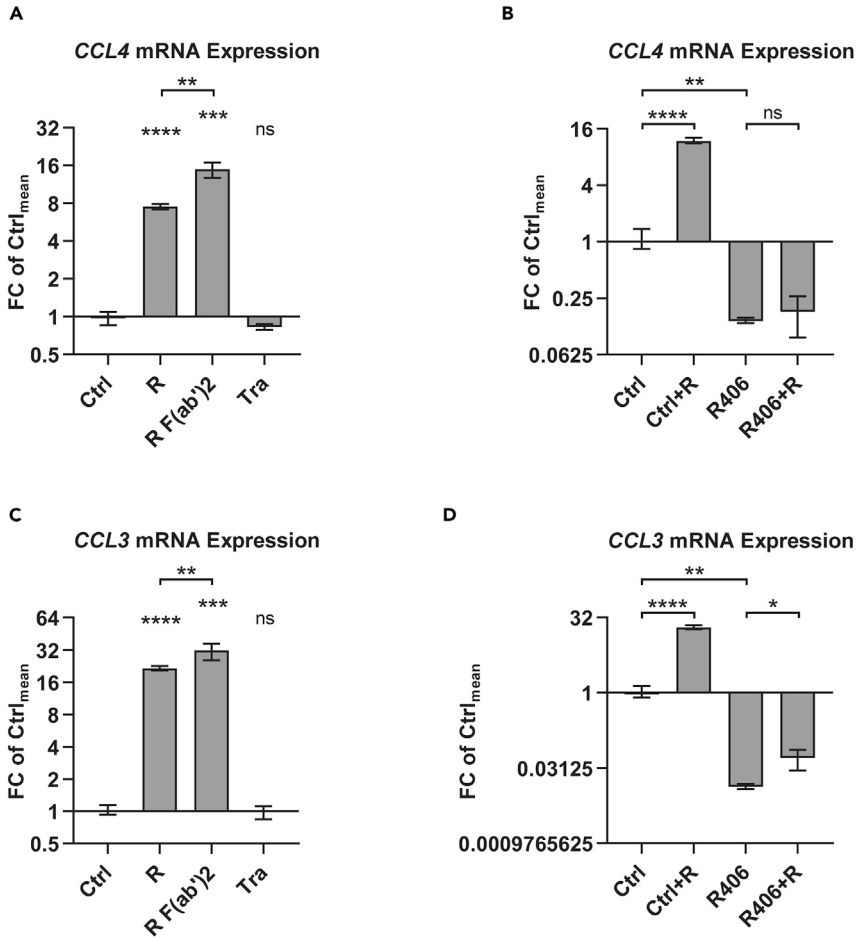

Figure 1. Rituximab activates B cell receptor signaling as inferred by *CCL4* and *CCL3* expression

(A–D) *CCL4* (A + B) and *CCL3* (C + D) expression was assessed in SU-DHL4 cells by qRT-PCR after 150-min treatment with rituximab (R), rituximab F(ab')$_2$ fragments (R F(ab')$_2$), or with trastuzumab (Tra) relative to untreated control samples (Ctrl). Where applicable (B + D), cells were treated with the SYK inhibitor R406 or with DMSO vehicle control (Ctrl) for 48 h. Statistical significance was tested by unpaired parametric t tests based on 3 biological replicates for each treatment condition. Mean with range is plotted. *p<0.05, **p<0.01, ***p<0.001, ****p<0.0001, ns = not significant, as calculated by unpaired non-parametric t tests.

short-lived transcription factor (Figure 3B). In the absence of pro-survival stimuli, strong MYC activation can re-enforce apoptosis induction (Hoffman and Liebermann, 2008).

SYK kinase activity was not significantly altered, although rituximab or obinutuzumab treatment increased the phosphorylation level of 11 and 9 SYK residues, respectively. The phosphorylation sites included SYK Tyr^{352} but not SYK Tyr$^{525/526}$ located in the kinase activation loop (Figures 4A and S2). This constellation of phosphorylated Syk residues has previously been associated with B cell apoptosis (Muschen, 2018). We confirmed a lack of SYK Tyr$^{525/526}$ phosphorylation after obinutuzumab treatment by immunoblotting, but revealed low levels of SYK Tyr$^{525/526}$ phosphorylation by rituximab (Figure 4B).

Activation of the lipid kinase phosphatidylinositol 3-kinase (PI3K) was inferred by changes in the phosphorylation level of PI3K binding sites on CD19 and BCAP and by activity changes of downstream PI3K effectors (Werner et al., 2010). Increased tyrosine phosphorylation levels on CD19 and BCAP implied PI3K activation by rituximab as well as obinutuzumab, whereby more pronounced phosphorylation on CD19 Tyr^{500} after rituximab was suggestive of stronger PI3K activation following this treatment (Figure S3). However, of the three PI3K effectors MTOR, PDK1, and AKT, only AKT was found to be more active at the 1 h time point after rituximab treatment (Figure 2), likely resulting from direct AKT activation by Ca^{2+} flux following

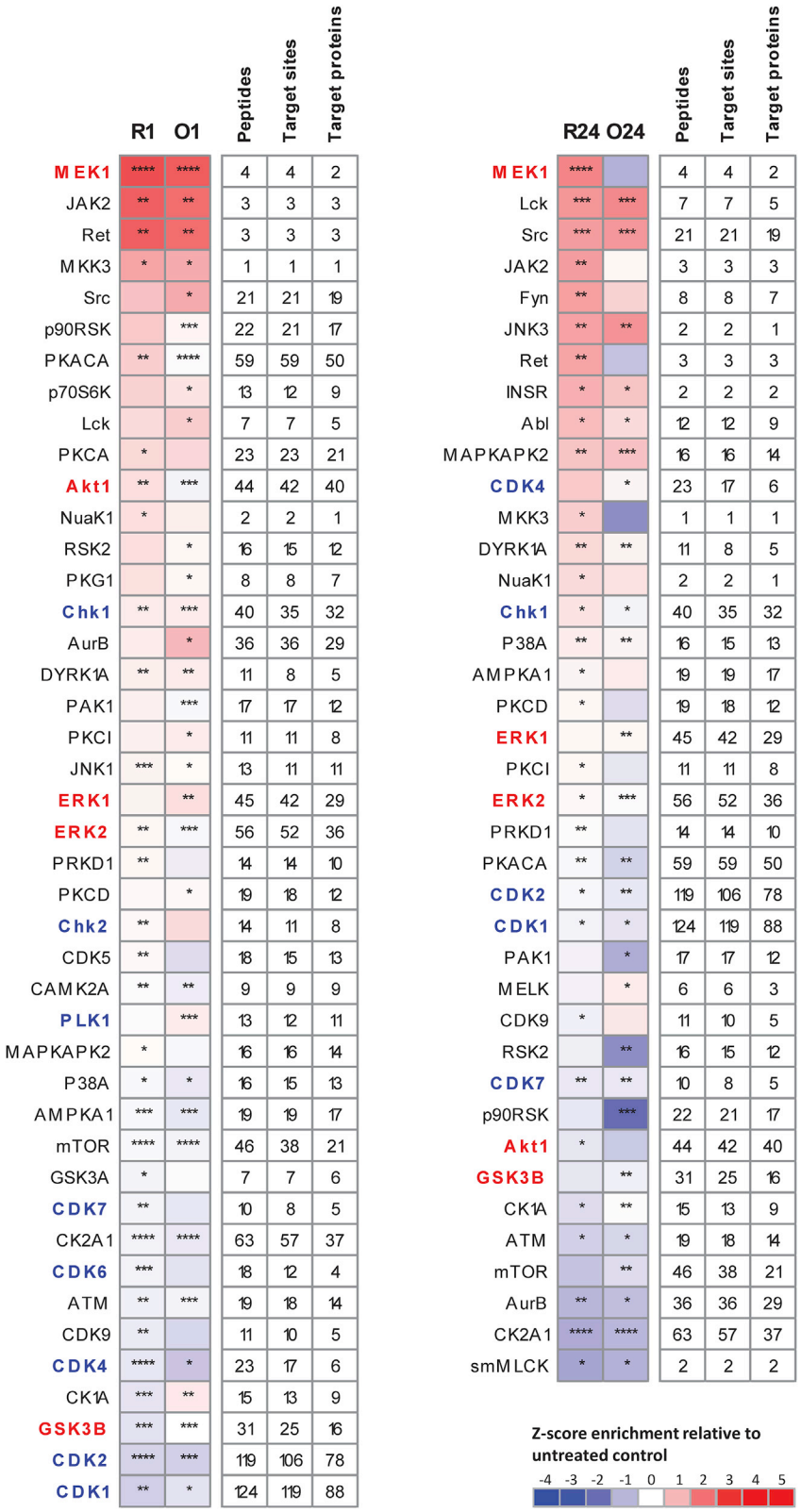
R1
O1
Peptides
Target sites
Target proteins
MEK1 **** **** 4 4 2
JAK2 ** ** 3 3 3
Ret ** ** 3 3 3
MKK3 * * 1 1 1
Src * 21 21 19
p90RSK *** 22 21 17
PKACA ** **** 59 59 50
p70S6K * 13 12 9
Lck * 7 7 5
PKCA * 23 23 21
Akt1 ** *** 44 42 40
NuaK1 * 2 2 1
RSK2 * 16 15 12
PKG1 * 8 8 7
Chk1 ** *** 40 35 32
AurB * 36 36 29
DYRK1A ** ** 11 8 5
PAK1 *** 17 17 12
PKCI * 11 11 8
JNK1 *** * 13 11 11
ERK1 ** 45 42 29
ERK2 ** *** 56 52 36
PRKD1 ** 14 14 10
PKCD * 19 18 12
Chk2 ** 14 11 8
CDK5 ** 18 15 13
CAMK2A ** ** 9 9 9
PLK1 *** 13 12 11
MAPKAPK2 * 16 16 14
P38A * * 16 15 13
AMPKA1 *** *** 19 19 17
mTOR **** **** 46 38 21
GSK3A * 7 7 6
CDK7 ** 10 8 5
CK2A1 **** **** 63 57 37
CDK6 *** 18 12 4
ATM ** *** 19 18 14
CDK9 ** 11 10 5
CDK4 **** * 23 17 6
CK1A *** ** 15 13 9
GSK3B *** *** 31 25 16
CDK2 **** *** 119 106 78
CDK1 ** * 124 119 88
R24
O24
Peptides
Target sites
Target proteins
MEK1 **** 4 4 2
Lck *** *** 7 7 5
Src *** *** 21 21 19
JAK2 ** 3 3 3
Fyn ** 8 8 7
JNK3 ** ** 2 2 1
Ret ** 3 3 3
INSR * * 2 2 2
Abl * * 12 12 9
MAPKAPK2 ** *** 16 16 14
CDK4 * 23 17 6
MKK3 * 1 1 1
DYRK1A ** ** 11 8 5
NuaK1 * 2 2 1
Chk1 * * 40 35 32
P38A ** ** 16 15 13
AMPKA1 * 19 19 17
PKCD * 19 18 12
ERK1 ** 45 42 29
PKCI * 11 11 8
ERK2 * *** 56 52 36
PRKD1 ** 14 14 10
PKACA ** ** 59 59 50
CDK2 * ** 119 106 78
CDK1 * * 124 119 88
PAK1 * 17 17 12
MELK * 6 6 3
CDK9 * 11 10 5
RSK2 ** 16 15 12
CDK7 ** ** 10 8 5
p90RSK *** 22 21 17
Akt1 * 44 42 40
GSK3B ** 31 25 16
CK1A * ** 15 13 9
ATM * * 19 18 14
mTOR ** 46 38 21
AurB ** * 36 36 29
CK2A1 **** **** 63 57 37
smMLCK * * 2 2 2
Z-score enrichment relative to untreated control
-4 -3 -2 -1 0 1 2 3 4 5

Figure 2. Kinase activity changes after rituximab or obinutuzumab treatment

SU-DHL4 cells were treated with 5 μg/mL rituximab (R) or obinutuzumab (O) for 1 h (R1 and O1; left) or 24 h (R24 and O24; right), and changes in kinase activities were inferred relative to untreated controls. The heatmaps show the *Z* score enrichment of substrate groups for the different kinases calculated by the KSEA algorithm. Kinases belonging to the KEGG pathway "B-cell receptor signaling" are indicated in red, and those belonging to the KEGG pathway "cell cycle" are indicated in blue. Peptides: number of peptides containing a phosphorylation site regulated by respective kinase; Target sites: number of phosphorylation sites measured for respective kinase; Target proteins: number of proteins that the phosphorylation sites regulated by the respective kinase map to. *p<0.05, **p<0.01, ***p<0.001, ****p<0.0001 as inferred by the hypergeometric test followed by Benjamini-Hochberg multiple testing correction.

treatment with type I but not type II anti-CD20 monoclonal antibodies (Walshe et al., 2008; Yano et al., 1998). To validate AKT activation we assessed phosphorylation of AKT Thr^{308} and Ser^{473} by immunoblotting due to lack of evidence in our LC-MS/MS data. Although AKT Thr^{308} phosphorylation was not observed (data not shown), we found a strong increase in AKT Ser^{473} phosphorylation at 1 h after rituximab and rituximab F(ab')$_2$ treatment with fading signals at the 24 h time point (Figure S4). This result corresponded with phosphorylation of the AKT target site PRAS40 Thr^{246}. Only low levels of phospho-AKT Ser^{473} were detected after obinutuzumab treatment and no increase in AKT Ser^{473} phosphorylation was observed after isotype control trastuzumab treatment (Figure 5A).

Because of the known powerful pro-survival effects of AKT (Werner et al., 2010), the differing ability of rituximab and obinutuzumab to activate this kinase constituted a decisive difference between the two monoclonal antibodies at the molecular level. Consistently, BAD Ser^{99}, as an important AKT target site with key role in inhibition of apoptosis, was found phosphorylated only after rituximab treatment ($p = 0.024$; 1 h). In addition, rituximab more than obinutuzumab increased levels of Ser^{118} phosphorylation on BAD ($p = 0.0074$ at 1 h; $p = 0.0007$ at 24 h; Figure 5B). Phosphorylation on Ser^{99} and Ser^{118} sequesters pro-apoptotic BAD in the cytosol and impairs its inhibitory effects on anti-apoptotic BCL2 and BCL-xL so that rituximab more than obinutuzumab may diminish direct B cell death by reinforcing BCL2-mediated anti-apoptotic signals (Masters et al., 2001; Zha et al., 1996). In line with this notion, SU-DHL4 cell viability was more strongly decreased by obinutuzumab than rituximab treatment (Alduaij et al., 2011; Herter et al., 2013).

Links between BCR and NOTCH1 signaling

We next sought to understand the link between rituximab treatment and NOTCH1 signaling. Based on publications showing increased ADAM activity upon Ca^{2+} flux and PI3K/MAPK-dependent phosphorylation changes (Herzog et al., 2014; Fan et al., 2003; Zhang et al., 2006; Li et al., 2018), we hypothesized that anti-CD20 monoclonal antibodies could enhance ADAM10/ADAM17-mediated NOTCH1 cleavage. To quantify short-term rises of NOTCH1 signaling, we assessed expression changes of its target gene *HES1* by qRT-PCR. Results obtained for rituximab and its control antibodies in SU-DHL4 cells correlated with BCR activation after rituximab treatment, as demonstrated by *CCL4* expression (Figure 6A). An increase in *HES1* expression after rituximab treatment was also validated in primary CLL cells (Figure S5).

The increases in *HES1* expression observed after rituximab treatment in SU-DHL4 cells matched those induced by SB2H2 treatment, which cross-links and activates the IgG BCR of SU-DHL4 directly (Figure 6B). Abolishment of Ca^{2+} flux and BCR signaling by R406 completely abrogated the increase in *HES1* and *CCL4* expression after rituximab exposure (Figure 6C). Treatment with the PI3K inhibitor idelalisib and the BTK inhibitor ibrutinib clearly reduced nuclear NICD1 protein levels without obvious difference between both drugs (Figure 6D), but did not prevent the increase in *HES1* expression after rituximab treatment (Figure S6).

Direct comparison of rituximab and obinutuzumab treatments in SU-DHL4 cells revealed a much subtler increase in *HES1* expression following obinutuzumab treatment despite a comparable increase in *CCL4* expression (Figure 7A). This result was consistent with a role for Ca^{2+} flux during NOTCH1 activation (Le Gall et al., 2009; Arruga et al., 2020). In addition, LC-MS/MS data revealed significant de-phosphorylation of ADAM17 Ser^{791} only after rituximab treatment ($p=0.048$; Figure 7B), which has been shown previously to enhance the activity of ADAM17 (Fan et al., 2003). The kinetics of ADAM17 Ser^{791} de-phosphorylation followed those observed in the PI3K/AKT pathway suggesting positive feedback from this pathway to the NOTCH1 receptor.

We finally validated NOTCH1 activation by rituximab at protein level. Western blot analysis for NICD1 showed increased NOTCH1 signaling after rituximab treatment in SU-DHL4 cells and three independent

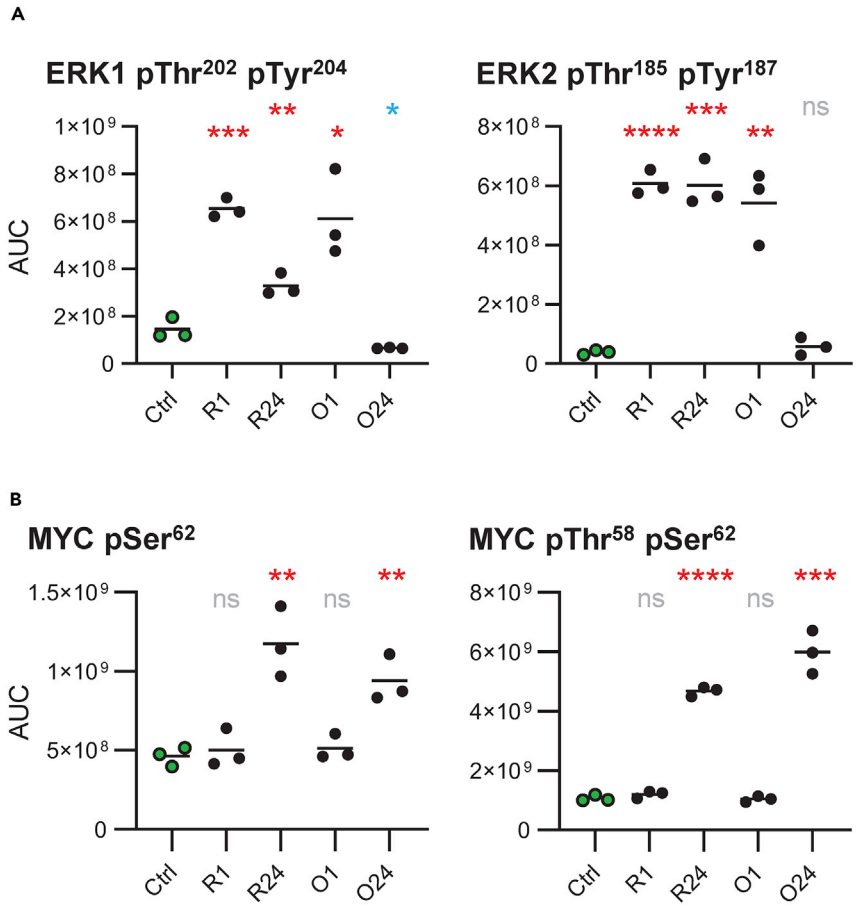

Figure 3. Rituximab and obinutuzumab induce ERK and MYC phosphorylation capable to induce B cell death

(A) Calculated areas under the curve (AUC) for phosphopeptide ions dually phosphorylated on ERK1 Thr^{202}/Tyr^{204} (left) and on ERK2 Thr^{185}/Tyr^{187} (right) after treatment with rituximab (R) or obinutuzumab (O) for 1 or 24 h. Each of the three plotted biological replicates depict the average of the two analytical replicates. Phosphorylation changes were tested for statistical significance by unpaired non-parametric t tests calculated toward untreated control samples (Ctrl). Significant phosphorylation is indicated in red; significant de-phosphorylation is indicated in blue.

(B) Calculated AUCs for phosphopeptide ions phosphorylated on MYC Ser^{62} (left) and dually phosphorylated on MYC Thr^{58}/Ser^{62} (right).

Line indicates mean. *p<0.05, **p<0.01, ***p<0.001, ****p<0.0001, ns = not significant, as calculated by unpaired non-parametric t tests.

CLL cases (Figure S7). However, increased NOTCH1 signaling after treatment with rituximab $F(ab')_2$ fragments was inconsistently observed in primary CLL cells. This may be afforded by heterogeneous basal activity levels of the NOTCH1 receptor as well as in the B cell receptor signaling cascade. In contrast to results obtained with the SU-DHL4 cell line, trastuzumab treatment increased NOTCH1 cleavage in all three primary CLL samples. Trastuzumab binds to the Fc gamma receptor expressed on immune effector cells, and we hence reasoned that in addition to B cell-intrinsic modes of NOTCH1 activation, cleavage of NOTCH1 may, furthermore, be enhanced by effector cell activation. To address this hypothesis, we correlated the increase in *HES1* expression in eight independent CLL samples with the respective increase in *CCL2* expression (Figure S8). The latter was used as a surrogate marker for the presence of activated monocytes (Schulz et al., 2011). Our results supported a positive correlation between the extent of monocyte activation and NOTCH1 signaling strength ($R2=0.79$; $p<0.0001$), which may result from a recruitment of NOTCH1 ligand expressing monocytes to CLL cells and/or from an activation of B cell-intrinsic signaling pathways subsequent to a release of signaling molecules into the culture medium by activated effector cells (Lopez-Guerra et al., 2020).

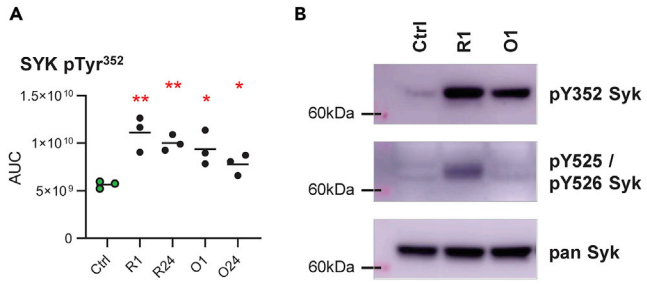

Figure 4. Obinutuzumab exceeds rituximab in supporting apoptosis induction by means of aberrant SYK phosphorylation.

(A) Calculated AUCs for phosphopeptide ions containing the phosphorylation site Tyr^{352} on SYK. Line indicates mean. *p<0.05, **p<0.01, as calculated by unpaired non-parametric t tests.

(B) Immunoblot detection of phospho-SYK Tyr^{352} and phospho-SYK Tyr^{525}/Tyr^{526} in SU-DHL4 cells treated with 2.5 μg/ml rituximab (R) or obinutuzumab (O) for 1 h relative to untreated control samples (Ctrl; shown are representative results from one of four experiments).

Discussion

Our results demonstrate that rituximab and obinutuzumab both hijack the BCR signaling cascade, but in different directions. Excessive ERK and MYC activation by riyuximab and obinutuzumab treatment supported the hypothesis that both anti-CD20 monoclonal antibodies induce direct cell killing via signals generated in the BCR signaling cascade (Muschen, 2018; Hoffman and Liebermann, 2008). However, as demonstrated by an aberrant SYK phosphorylation pattern, obinutuzumab more effectively shifted the balance of these signals toward death, whereas rituximab engaged stronger signals associated with survival, comprising pro-survival SYK $Tyr^{525/526}$ phosphorylation, AKT activation, BAD Ser^{99} and Ser^{118} phosphorylation, and NOTCH1 activation. The stronger activation of NOTCH1 by rituximab acts in concert with AKT activation, because *BCL2* is a target gene of the NICD1 transcription factor and up-regulated *BAD* transcription has been observed in CLL with overactive NOTCH1 signaling (Fabbri et al., 2017). Hence, it appears that rituximab can reinforce BCL2-mediated apoptotic resistance at both the protein and gene expression levels thereby diminishing the degree of B cell killing (Werner et al., 2010; Fabbri et al., 2017). PEST-domain *NOTCH1* mutations therefore should reinforce pro-survival signals after rituximab treatment due to their activating effect on NICD1 potentially explaining the reduced benefit of adding rituximab to chemotherapy in *NOTCH1* mutant CLL (Stilgenbauer et al., 2014; Weng et al., 2004).

Clinical trial data suggest that our results could influence clinical practice. CLL and follicular lymphoma, which benefit from the use of obinutuzumab, are both characterized by high-level BCL2 expression (Goede et al., 2014, 2015; Marcus et al., 2017), whereas DLBCL is a more heterogeneous entity (Schmitz et al., 2018). Focusing on germinal center B cell-type DLBCL encompassing a considerable number of cases with genetic alterations affecting BCL2 family members revealed a trend toward PFS improvement using obinutuzumab (Vitolo et al., 2017; Schmitz et al., 2018). In contrast, PFS analysis within the activated B cell (ABC-)type DLBCL showed almost identical results for both treatment arms, which may be afforded by frequent co-occurrence of genetic aberrations affecting BCL2 family members with those affecting proximal BCR signaling (Vitolo et al., 2017; Schmitz et al., 2018). The latter have been associated with chronic active BCR signaling bringing about a lower capacity for rituximab and obinutuzumab to alter intrinsic B cell signals (Schmitz et al., 2018), hence likely reducing the molecular advantages observed for obinutuzumab. Considering these observations, our results warrant refined analyses of respective trial cohorts to identify biomarkers indicating where obinutuzumab should become standard of care in the treatment of B cell lymphoma.

BCR signaling is a driver of lymphomagenesis (Niemann and Wiestner, 2013) to the extent that its activation bears the risk of providing growth stimuli to lymphoma cells if the apoptotic threshold is not reached. This risk is higher using rituximab, which may be reflected in loss of CD20 expression at relapse post rituximab treatment if lymphoma cells fail to reach the threshold because of (ultra-)low CD20 expression (Hiraga et al., 2009; Tomita, 2016). Moreover, the increase in BCR signaling after anti-CD20 treatment interacts with the modes of action of concomitant drugs. Response to cell cycle-dependent cytostatic agents may be reduced by an arrest in the cell cycle, and targeting CD20 as well as BTK may lead to partial antagonization of each other's effects, providing a rationale for the lack of PFS

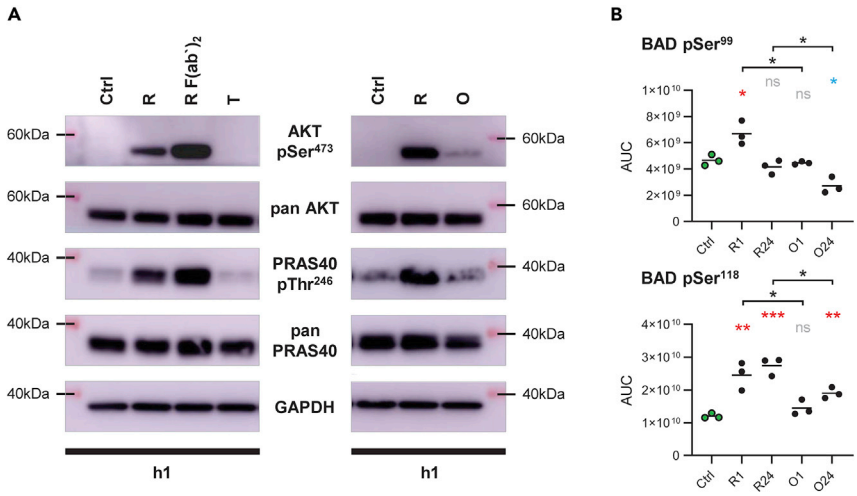

Figure 5. Rituximab more than obinutuzumab induces pro-survival signals

(A) Immunoblot detection of phospho-AKT Ser^{473} and phospho-PRAS40 Thr^{246} in SU-DHL4 cells treated with 2.5 μg/ml rituximab (R), rituximab F(ab')$_2$ fragments (R F(ab')$_2$), trastuzumab (T), or obinutuzumab (O) for 1 h relative to untreated control samples (Ctrl). Shown are representative results from one of four experiments.

(B) Calculated AUCs for phosphopeptide ions containing the phosphorylation site Ser^{99} (top) or Ser^{118} (bottom) on BAD. Line indicates mean. *p<0.05, **p<0.01, ***p<0.001, ns = not significant, as calculated by unpaired non-parametric t tests.

improvement observed in CLL after adding rituximab to ibrutinib treatment (Burger et al., 2019). In contrast, PI3K and BCL2 inhibitors likely exert complementary effects on anti-CD20 therapy. Our results thus provide new explanatory approaches for therapy resistance in B cell lymphoma treatment and help to refine patient selection for rituximab or obinutuzumab and to improve drug sequencing within anti-CD20 monoclonal antibody containing treatment protocols.

Furthermore, we identify the membrane-bound transcription factor NOTCH1 as a connective link between the BCR signaling cascade and genes promoting B cell survival and proliferation. NOTCH1 cleavage upon Ca^{2+} flux allows rapid NICD1 release after BCR activation, and modulation of ADAM17 cleavage activity by (de-) phosphorylation allows an adjustment of NOTCH1 signaling strength. ADAM10 was shown to cleave NOTCH1 after ligand binding, whereas ADAM17 has been associated with ligand-independent NOTCH1 activation (Bozkulak and Weinmaster, 2009). Activation of ADAM17 by signals generated through an (auto-)active BCR may therefore explain high NICD1 protein levels observed in *NOTCH1* wild-type peripheral blood CLL cells that lack contact to NOTCH1 ligands (Fabbri et al., 2017). Moreover, our data suggest that NOTCH1 cleavage in B cells is also dependent on the level of immune effector cell activation in the microenvironment allowing an adaption of NOTCH1 signaling in B cells to the degree of inflammation. Taken together, our results warrant more detailed studies aiming at a better understanding of ADAM10/17 regulation in B cells to exploit the underlying mechanisms for effective suppression of NOTCH1 signaling.

In conclusion, our results demonstrate unexpected complexity by which rituximab and obinutuzumab interfere with signaling pathways essential for B cell lymphoma pathogenesis and treatment. This new insight provides impetus to better personalize the choice of rituximab or obinutuzumab for anti-CD20 treatment, to optimize the design of protocols encompassing anti-CD20 monoclonal antibodies, and to develop new strategies for the treatment of NOTCH1-driven B cell lymphoma.

Limitations of study

A limitation of the study is that B cell-intrinsic signaling processes after anti-CD20 treatment have been determined in one cell line only and that the results obtained therefore lack evidence for general applicability. The work is hypothesis generating and paves the way toward subsequent studies addressing each conclusion drawn.

Resource availability

Lead contact

Jennifer Edelmann, MD, PhD.

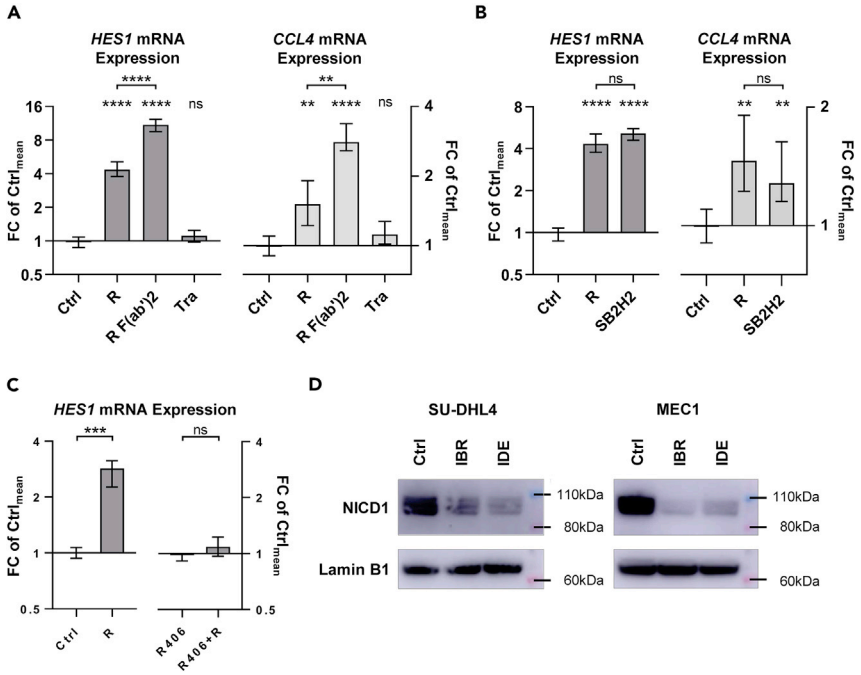

Figure 6. NOTCH1 and BCR signaling are synergized

(A) *HES1* (left) and *CCL4* (right) expression was assessed in SU-DHL4 cells by qRT-PCR after 150 min treatment with 2.5 μg/ml rituximab (R), rituximab F(ab')2 fragments (R F(ab')$_2$), or trastuzumab (T) relative to untreated control samples (Ctrl). Statistical significance was tested by unpaired non-parametric t tests based on 8 biological replicates for the control samples and 4 biological replicates for each treatment condition.

(B) *HES1* and *CCL4* expression in SU-DHL4 cells after 150 min of treatment with 2.5 μg/ml rituximab (R) or SB2H2 relative to untreated control samples (Ctrl).

(C) *HES1* expression in SU-DHL4 cells pre-treated with vehicle control (Ctrl, left) or R406 (5 μM; right) before treatment with 2.5 μg/mL rituximab (R) for 150 min.

(D) Immunoblot detection of nuclear NICD1 protein levels in SU-DHL4 cells (left) and MEC1 cells (right) after 48 h treatment with ibrutinib (IBR; 1 μM) or idelalisib (IDE; 5 μM) relative to samples treated with vehicle control (Ctrl). Shown are representative results for one of four experiments on SU-DHL4 cells and one of two experiments on MEC1 cells. Mean with range is plotted. *p<0.05, **p<0.01, ***p<0.001, ****p<0.0001, ns = not significant, as calculated by unpaired non-parametric t tests.

Department of Internal Medicine III, Ulm University, Albert-Einstein-Allee 23, 89,081 Ulm, Germany.

Mail: jennifer.edelmann@uni-ulm.de.

Tel: +49 (0)731 500 45849.

Materials availability

This study did not generate new unique reagents.

Data and code availability

The mass spectrometry proteomics data generated during this study have been deposited to the ProteomeXchange Consortium via the PRIDE partner repository with the dataset identifier PXD023572 and 10.6019/PXD023572.

METHODS

All methods can be found in the accompanying Transparent Methods supplemental file.

SUPPLEMENTAL INFORMATION

Supplemental Information can be found online at https://doi.org/10.1016/j.isci.2021.102089.

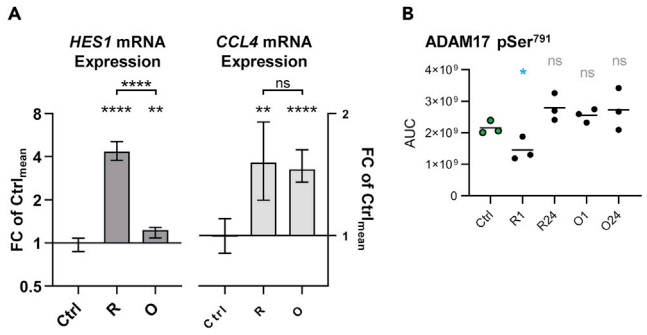

Figure 7. Rituximab induces NOTCH1 signaling more strongly than obinutuzumab

(A) *HES1* (left) and *CCL4* (right) expression in SU-DHL4 cells after 150 min of treatment with 2.5 μg/ml rituximab (R) or obinutuzumab (O) relative to untreated controls (Ctrl). Mean with range is plotted.

(B) Calculated AUCs for phosphopeptide ions containing the phosphorylation site Ser^{791} on ADAM17. Line indicates mean. *p<0.05, **p<0.01, ***p<0.001, ****p<0.0001ns = not significant, as calculated by unpaired non-parametric t tests.

ACKNOWLEDGMENTS

We thank Sameena Iqubal and Janet Matthews from Barts Cancer Institute for their help with the acquisition of primary CLL samples, Ryan Smith from Barts Cancer Institute for his help with the analysis of LC-MS/MS raw data, Graham Packham and Stephen Beers from Southampton University for helpful discussions, and Doriana di Bella from Barts Cancer Institute for her assistance with experiments.

The study was supported by the German Research Foundation (ED 256/1-1), the Barts Charity Fund, NIH (NCI PO1 CA81534), the Barry Reed Cancer Research Fund, and the Clinician Scientist Program of the Medical Faculty, Ulm University.

AUTHOR CONTRIBUTIONS

All authors contributed extensively to the work presented in this paper. J.E. designed research; performed, analyzed, and interpreted experiments; and wrote the paper. A.D.D. designed and performed the LC-MS/MS experiment, analyzed the raw data, and contributed to interpretation of the LC-MS/MS experiment. E.V. designed and performed the LC-MS/MS experiment. K.H. analyzed experimental data. M.C. and A.B. contributed to research design and data interpretation. H.D. contributed to data interpretation. P.C. contributed to design, analysis, and interpretation of the LC-MS/MS experiment. J.G.G. contributed to research design and interpretation. All authors contributed to write the paper.

DECLARATION OF INTERESTS

A.D.D. is Senior Scientist at Kinomica Ltd.

E.V. is employed by The Janssen Pharmaceutical Companies of Johnson & Johnson.

D.B. is Academic Funder and CSO at Kinomica Ltd.

M.C. acts as a consultant for a number of biotech companies, being retained as a consultant for BioInvent and has received research funding from BioInvent, GSK, UCB, iTeos, and Roche.

P.C. is Academic Funder and Director at Kinomica Ltd.

Disclosures J.G.G.: Janssen: Advisory Board, Honoraria, Research funding; Acerta: Advisory Board, Honoraria, Research funding; Celgene: Advisory Board, Honoraria, Research funding; Kite: Advisory Board, Honoraria; AbbVie: Advisory Board, Honoraria; Novartis: Advisory Board; TG Therapeutics: Advisory Board.

Disclosures H.D.: Abbvie: Consultancy, Honoraria; Agios: Consultancy, Honoraria, Research funding; Amgen: Consultancy, Honoraria, Research Funding; AROG: Research funding; Astellas: Consultancy, Honoraria, Research funding; Astex: Consultancy, Honoraria; Bristol Myers Squibb: Consultancy, Honoraria,

Research Funding; Celgene: Consultancy, Honoraria, Research funding; Janssen: Consultancy, Honoraria; Jazz: Consultancy, Honoraria, Research Funding; Helsinn: Consultancy, Honoraria; Novartis: Consultancy, Honoraria, Research funding; Oxford Biomedicals: Consultancy, Honoraria; Pfizer: Research funding; Roche: Consultancy, Honoraria; Sunesis: Research funding; AstraZeneca: Consultancy, Honoraria; GEM-oaB: Consultancy, Honoraria.

The remaining authors declare no competing interests.

Received: July 1, 2020
Revised: September 17, 2020
Accepted: January 18, 2021
Published: February 19, 2021

REFERENCES

Alduaij, W., Ivanov, A., Honeychurch, J., Cheadle, E.J., Potluri, S., Lim, S.H., Shimada, K., Chan, C.H., Tutt, A., Beers, S.A., et al. (2011). Novel type II anti-CD20 monoclonal antibody (GA101) evokes homotypic adhesion and actin-dependent, lysosome-mediated cell death in B-cell malignancies. Blood *117*, 4519–4529.

Arruga, F., Bracciama, V., Vitale, N., Vaisitti, T., Gizzi, K., Yeomans, A., Coscia, M., D'arena, G., Gaidano, G., Allan, J.N., et al. (2020). Bidirectional linkage between the B-cell receptor and NOTCH1 in chronic lymphocytic leukemia and in Richter's syndrome: therapeutic implications. Leukemia *34*, 462–477.

Borggrefe, T., and Oswald, F. (2009). The Notch signaling pathway: transcriptional regulation at Notch target genes. Cell. Mol. Life Sci. *66*, 1631–1646.

Bozkulak, E.C., and Weinmaster, G. (2009). Selective use of ADAM10 and ADAM17 in activation of Notch1 signaling. Mol. Cell. Biol. *29*, 5679–5695.

Burger, J.A., Sivina, M., Jain, N., Kim, E., Kadia, T., Estrov, Z., Nogueras-Gonzalez, G.M., Huang, X., Jorgensen, J., Li, J., et al. (2019). Randomized trial of ibrutinib vs ibrutinib plus rituximab in patients with chronic lymphocytic leukemia. Blood *133*, 1011–1019.

Estenfelder, S., Tausch, E., Robrecht, S., Bahlo, J., Goede, V., Ritgen, M., van Dongen, J.J.M., Langerak, A.W., Fingerle-Rowson, G., Kneba, M., et al. (2016). Gene mutations and treatment outcome in the context of chlorambucil (clb) without or with the addition of rituximab (R) or obinutuzumab (GA-101, G) - results of an extensive analysis of the phase III study CLL11 of the German CLL study group. Blood *128*, 3227.

Fabbri, G., Holmes, A.B., Viganotti, M., Scuoppo, C., Belver, L., Herranz, D., Yan, X.J., Kieso, Y., Rossi, D., Gaidano, G., et al. (2017). Common nonmutational NOTCH1 activation in chronic lymphocytic leukemia. Proc. Natl. Acad. Sci. U S A *114*, E2911–E2919.

Fabbri, G., Rasi, S., Rossi, D., Trifonov, V., Khiabanian, H., Ma, J., Grunn, A., Fangazio, M., Capello, D., Monti, S., et al. (2011). Analysis of the chronic lymphocytic leukemia coding genome: role of NOTCH1 mutational activation. J. Exp. Med. *208*, 1389–1401.

Fan, H., Turck, C.W., and Derynck, R. (2003). Characterization of growth factor-induced serine phosphorylation of tumor necrosis factor-alpha converting enzyme and of an alternatively translated polypeptide. J. Biol. Chem. *278*, 18617–18627.

Franke, A., Niederfellner, G.J., Klein, C., and Burtscher, H. (2011). Antibodies against CD20 or B-cell receptor induce similar transcription patterns in human lymphoma cell lines. PLoS One *6*, e16596.

Goede, V., Fischer, K., Busch, R., Engelke, A., Eichhorst, B., Wendtner, C.M., Chagorova, T., De La Serna, J., Dilhuydy, M.S., Illmer, T., et al. (2014). Obinutuzumab plus chlorambucil in patients with CLL and coexisting conditions. N. Engl. J. Med. *370*, 1101–1110.

Goede, V., Fischer, K., Engelke, A., Schlag, R., Lepretre, S., Montero, L.F., Montillo, M., Fegan, C., Asikanius, E., Humphrey, K., et al. (2015). Obinutuzumab as frontline treatment of chronic lymphocytic leukemia: updated results of the CLL11 study. Leukemia *29*, 1602–1604.

Herter, S., Herting, F., Mundigl, O., Waldhauer, I., Weinzierl, T., Fauti, T., Muth, G., Ziegler-Landesberger, D., Van Puijenbroek, E., Lang, S., et al. (2013). Preclinical activity of the type II CD20 antibody GA101 (obinutuzumab) compared with rituximab and ofatumumab in vitro and in xenograft models. Mol. Cancer Ther. *12*, 2031–2042.

Herzog, C., Haun, R.S., Ludwig, A., Shah, S.V., and Kaushal, G.P. (2014). ADAM10 is the major sheddase responsible for the release of membrane-associated meprin A. J. Biol. Chem. *289*, 13308–13322.

Hiraga, J., Tomita, A., Sugimoto, T., Shimada, K., Ito, M., Nakamura, S., Kiyoi, H., Kinoshita, T., and Naoe, T. (2009). Down-regulation of CD20 expression in B-cell lymphoma cells after treatment with rituximab-containing combination chemotherapies: its prevalence and clinical significance. Blood *113*, 4885–4893.

Hoffman, B., and Liebermann, D.A. (2008). Apoptotic signaling by c-MYC. Oncogene *27*, 6462–6472.

Le Gall, S.M., Bobe, P., Reiss, K., Horiuchi, K., Niu, X.D., Lundell, D., Gibb, D.R., Conrad, D., Saftig, P., and Blobel, C.P. (2009). ADAMs 10 and 17 represent differentially regulated components of a general shedding machinery for membrane proteins such as transforming growth factor alpha, L-selectin, and tumor necrosis factor alpha. Mol. Biol. Cell *20*, 1785–1794.

Li, R., Wang, T., Walia, K., Gao, B., and Krepinsky, J.C. (2018). Regulation of profibrotic responses by ADAM17 activation in high glucose requires its C-terminus and FAK. J. Cell Sci. *131*, jcs208629.

Lopez-Guerra, M., Xargay-Torrent, S., Fuentes, P., Roldan, J., Gonzalez-Farre, B., Rosich, L., Silkenstedt, E., Garcia-Leon, M.J., Lee-Verges, E., Gimenez, N., et al. (2020). Specific NOTCH1 antibody targets DLL4-induced proliferation, migration, and angiogenesis in NOTCH1-mutated CLL cells. Oncogene *39*, 1185–1197.

Marcus, R., Davies, A., Ando, K., Klapper, W., Opat, S., Owen, C., Phillips, E., Sangha, R., Schlag, R., Seymour, J.F., et al. (2017). Obinutuzumab for the first-line treatment of follicular lymphoma. N. Engl. J. Med. *377*, 1331–1344.

Marshall, M.J.E., Stopforth, R.J., and Cragg, M.S. (2017). Therapeutic antibodies: what have we learnt from targeting CD20 and where are we going? Front. Immunol. *8*, 1245.

Masters, S.C., Yang, H., Datta, S.R., Greenberg, M.E., and Fu, H. (2001). 14-3-3 inhibits Bad-induced cell death through interaction with serine-136. Mol. Pharmacol. *60*, 1325–1331.

Mossner, E., Brunker, P., Moser, S., Puntener, U., Schmidt, C., Herter, S., Grau, R., Gerdes, C., Nopora, A., Van Puijenbroek, et al.. (2010). Increasing the efficacy of CD20 antibody therapy through the engineering of a new type II anti-CD20 antibody with enhanced direct and immune effector cell-mediated B-cell cytotoxicity. Blood *115*, 4393–4402.

Muschen, M. (2018). Autoimmunity checkpoints as therapeutic targets in B cell malignancies. Nat. Rev. Cancer *18*, 103–116.

Niemann, C.U., and Wiestner, A. (2013). B-cell receptor signaling as a driver of lymphoma development and evolution. Semin. Cancer Biol. *23*, 410–421.

Pavlasova, G., Borsky, M., Svobodova, V., Oppelt, J., Cerna, K., Novotna, J., Seda, V., Fojtova, M., Fajkus, J., Brychtova, Y., et al. (2018). Rituximab primarily targets an intra-clonal BCR signaling

proficient CLL subpopulation characterized by high CD20 levels. Leukemia *32*, 2028–2031.

Rouge, L., Chiang, N., Steffek, M., Kugel, C., Croll, T.I., Tam, C., Estevez, A., Arthur, C.P., Koth, C.M., Ciferri, C., et al. (2020). Structure of CD20 in complex with the therapeutic monoclonal antibody rituximab. Science *367*, 1224–1230.

Santos, M.A., Sarmento, L.M., Rebelo, M., Doce, A.A., Maillard, I., Dumortier, A., Neves, H., Radtke, F., Pear, W.S., Parreira, L., et al. (2007). Notch1 engagement by Delta-like-1 promotes differentiation of B lymphocytes to antibody-secreting cells. Proc. Natl. Acad. Sci. U S A *104*, 15454–15459.

Schmitz, R., Wright, G.W., Huang, D.W., Johnson, C.A., Phelan, J.D., Wang, J.Q., Roulland, S., Kasbekar, M., Young, R.M., Shaffer, A.L., et al. (2018). Genetics and pathogenesis of diffuse large B-cell lymphoma. N. Engl. J. Med. *378*, 1396–1407.

Schulz, A., Toedt, G., Zenz, T., Stilgenbauer, S., Lichter, P., and Seiffert, M. (2011). Inflammatory cytokines and signaling pathways are associated with survival of primary chronic lymphocytic leukemia cells in vitro: a dominant role of CCL2. Haematologica *96*, 408–416.

Stilgenbauer, S., Schnaiter, A., Paschka, P., Zenz, T., Rossi, M., Dohner, K., Buhler, A., Bottcher, S., Ritgen, M., Kneba, M., et al. (2014). Gene mutations and treatment outcome in chronic lymphocytic leukemia: results from the CLL8 trial. Blood *123*, 3247–3254.

Takahashi, K., Sivina, M., Hoellenriegel, J., Oki, Y., Hagemeister, F.B., Fayad, L., Romaguera, J.E., Fowler, N., Fanale, M.A., Kwak, L.W., et al. (2015). CCL3 and CCL4 are biomarkers for B cell receptor pathway activation and prognostic serum markers in diffuse large B cell lymphoma. Br. J. Haematol. *171*, 726–735.

Tomita, A. (2016). Genetic and epigenetic modulation of CD20 expression in B-cell malignancies: molecular mechanisms and significance to rituximab resistance. J. Clin. Exp. Hematop. *56*, 89–99.

Vitolo, U., Trneny, M., Belada, D., Burke, J.M., Carella, A.M., Chua, N., Abrisqueta, P., Demeter, J., Flinn, I., Hong, X., et al. (2017). Obinutuzumab or rituximab plus cyclophosphamide, doxorubicin, vincristine, and prednisone in previously untreated diffuse large B-cell lymphoma. J. Clin. Oncol. *35*, 3529–3537.

Walshe, C.A., Beers, S.A., French, R.R., Chan, C.H., Johnson, P.W., Packham, G.K., Glennie, M.J., and Cragg, M.S. (2008). Induction of cytosolic calcium flux by CD20 is dependent upon B Cell antigen receptor signaling. J. Biol. Chem. *283*, 16971–16984.

Weng, A.P., Ferrando, A.A., Lee, W., Morris, J.P.T., Silverman, L.B., Sanchez-Irizarry, C., Blacklow, S.C., Look, A.T., and Aster, J.C. (2004). Activating mutations of NOTCH1 in human T cell acute lymphoblastic leukemia. Science *306*, 269–271.

Werner, M., Hobeika, E., and Jumaa, H. (2010). Role of PI3K in the generation and survival of B cells. Immunol. Rev. *237*, 55–71.

Yano, S., Tokumitsu, H., and Soderling, T.R. (1998). Calcium promotes cell survival through CaM-K kinase activation of the protein-kinase-B pathway. Nature *396*, 584–587.

Zha, J., Harada, H., Yang, E., Jockel, J., and Korsmeyer, S.J. (1996). Serine phosphorylation of death agonist BAD in response to survival factor results in binding to 14-3-3 not BCL-X(L). Cell *87*, 619–628.

Zhang, Q., Thomas, S.M., Lui, V.W., Xi, S., Siegfried, J.M., Fan, H., Smithgall, T.E., Mills, G.B., and Grandis, J.R. (2006). Phosphorylation of TNF-alpha converting enzyme by gastrin-releasing peptide induces amphiregulin release and EGF receptor activation. Proc. Natl. Acad. Sci. U S A *103*, 6901–6906.

iScience, Volume *24*

Supplemental Information

Rituximab and obinutuzumab differentially hijack the B cell receptor and NOTCH1 signaling pathways

Jennifer Edelmann, Arran D. Dokal, Emma Vilventhraraja, Karlheinz Holzmann, David Britton, Tetyana Klymenko, Hartmut Döhner, Mark Cragg, Andrejs Braun, Pedro Cutillas, and John G. Gribben

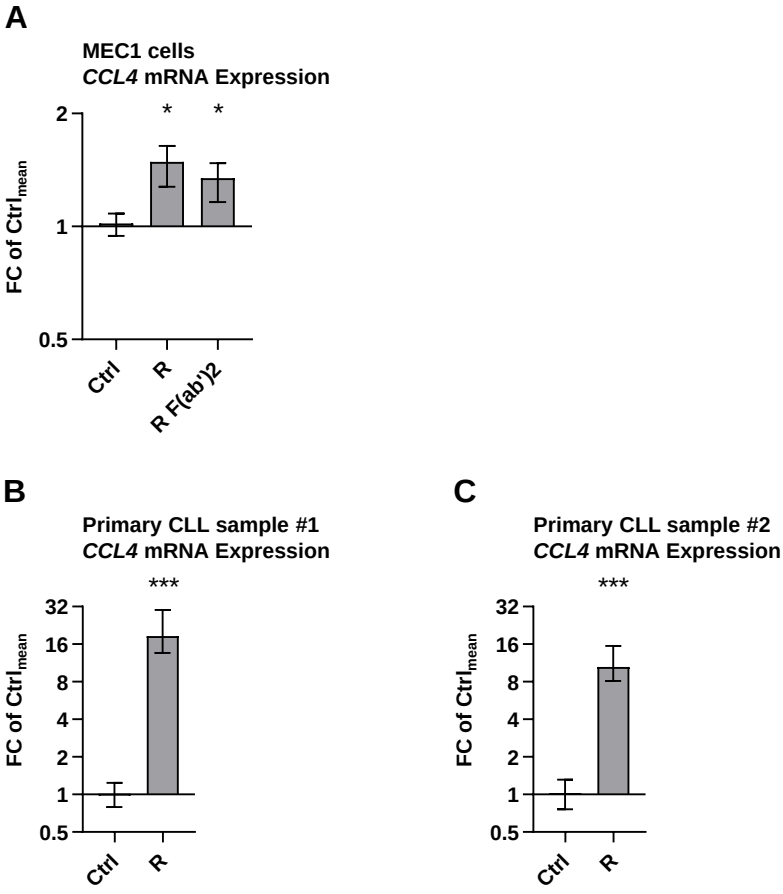

Supplementary Figure S1:

Validation of activated B-cell receptor signaling by rituximab treatment in MEC1 cells and two primary CLL samples.

Related to Figure 1.

CCL4 expression was assessed in MEC1 cells (**A**) and in primary CLL cells (**B** + **C**) after 150 minutes of treatment with rituximab (R) or rituximab F(ab')$_2$ fragments (R F(ab')$_2$) relative to untreated control samples (Ctrl). Statistical significance was tested by unpaired parametric t-tests based on 3 biological replicates for each treatment condition in the case of MEC1 cells and based on 5 biological replicates in the case of primary CLL samples. Mean with range is plotted. *<0.05, **<0.01, ***<0.001; as calculated by unpaired non-parametric t-tests.

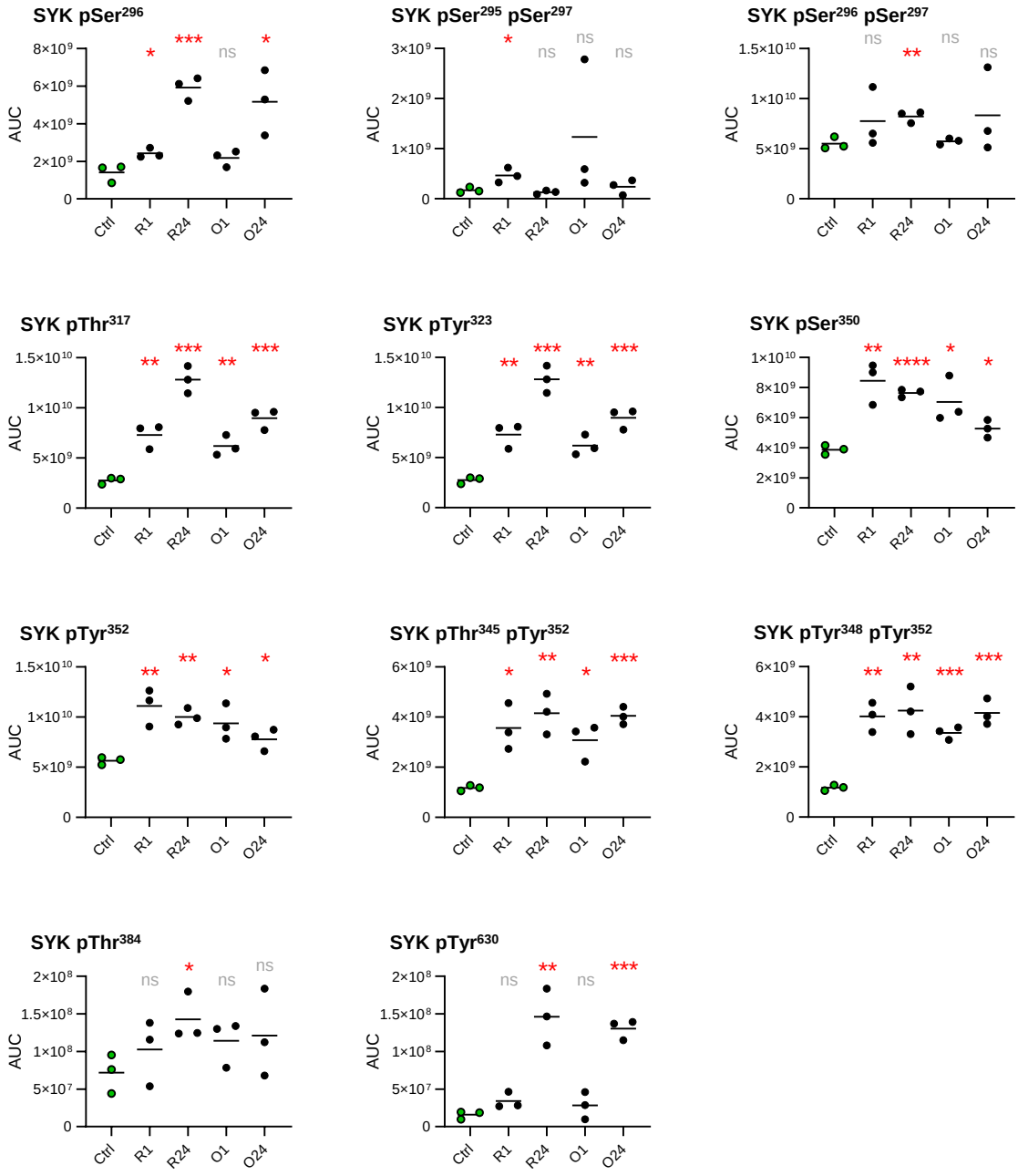

Supplementary Figure S2:

SYK phosphorylation after rituximab or obinutuzumab treatment.

Related to Figure 4.

Calculated AUCs for phosphopeptide ions containing the phosphorylation sites indicated above on SYK. Line indicates mean. *<0.05, **<0.01, ***<0.001, ns = not significant; as calculated by unpaired non-parametric t-tests.

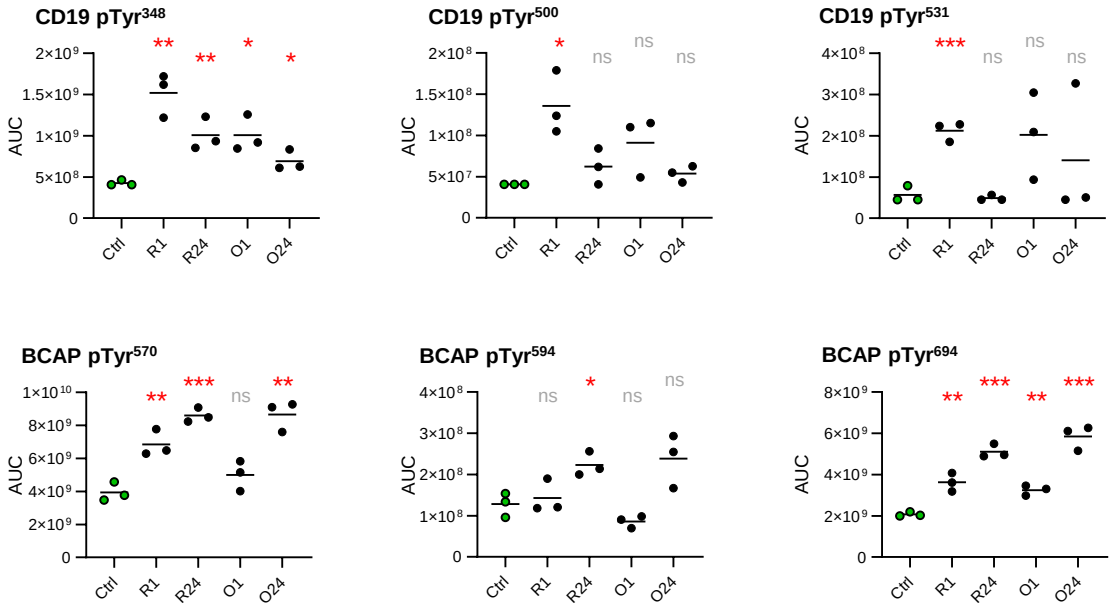

Supplementary Figure S3:

CD19 and BCAP phosphorylation after rituximab or obinutuzumab treatment.

Related to Figure 5.

Calculated AUCs for phosphopeptide ions containing the phosphorylation sites indicated above on CD19 (**top**) or BCAP (**bottom**). Line indicates mean. *<0.05, **<0.01, ***<0.001, ns = not significant; as calculated by unpaired non-parametric t-tests.

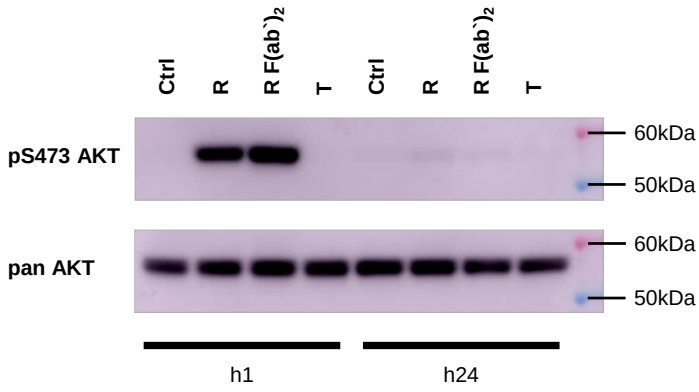

Supplementary Figure S4:

AKT activation was restricted to early time-points after rituximab treatment.

Related to Figure 5.

Immunoblot detection of phospho-AKT Ser^{473} in SU-DHL4 cells treated with rituximab (R), rituximab $F(ab')_2$ fragments (R $F(ab')_2$), or trastuzumab (T) for one hour (**left**) or 24 hours (**right**) relative to untreated control samples (Ctrl).

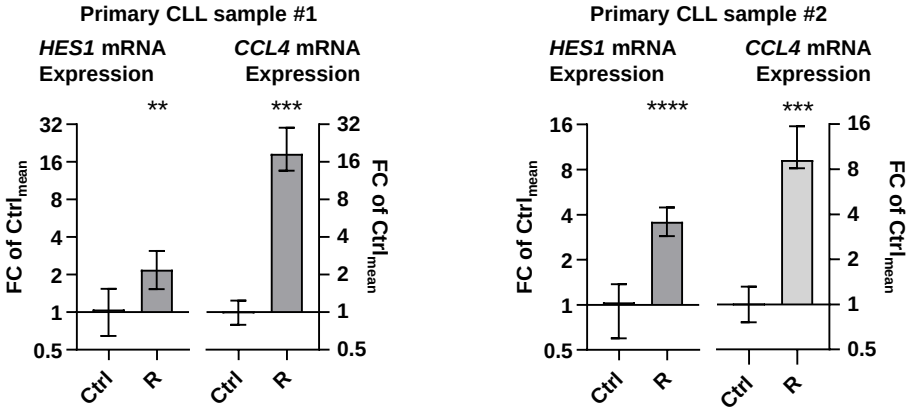

Supplementary Figure S5:

Validation of activated NOTCH1 signaling by rituximab treatment in two primary CLL samples.

Related to Figure 6.

HES1 and *CCL4* expression was assessed in primary CLL cells after 150 minutes of treatment with rituximab (R) relative to untreated control samples (Ctrl). Statistical significance was tested by unpaired parametric t-tests based on 5 biological replicates for each treatment condition. Mean with range is plotted. *<0.05, **<0.01, ***<0.001; as calculated by unpaired non-parametric t-tests.

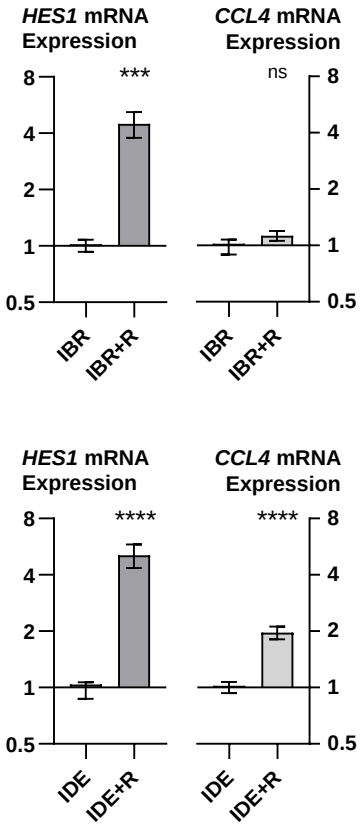

Supplementary Figure S6:

Treatment with ibrutinib or idelalisib did not prevent the increase in NOTCH1 signaling after rituximab treatment.

Related to Figure 6.

HES1 (**left**) and *CCL4* (**right**) expression was assessed in SU-DHL4 cells by qRT-PCR after 150 min of treatment with rituximab (R) relative to untreated control samples (Ctrl). Cells were pre-treated with the BTK inhibitor ibrutinib (**top**) or with the Pi3K inhibitor idelalisib (**bottom**) for 48 hours. Statistical significance was tested by unpaired parametric t-tests based on 4 biological replicates for each treatment condition. Mean with range is plotted. *<0.05, **<0.01, ***<0.001, ns = not significant; as calculated by unpaired non-parametric t-tests.

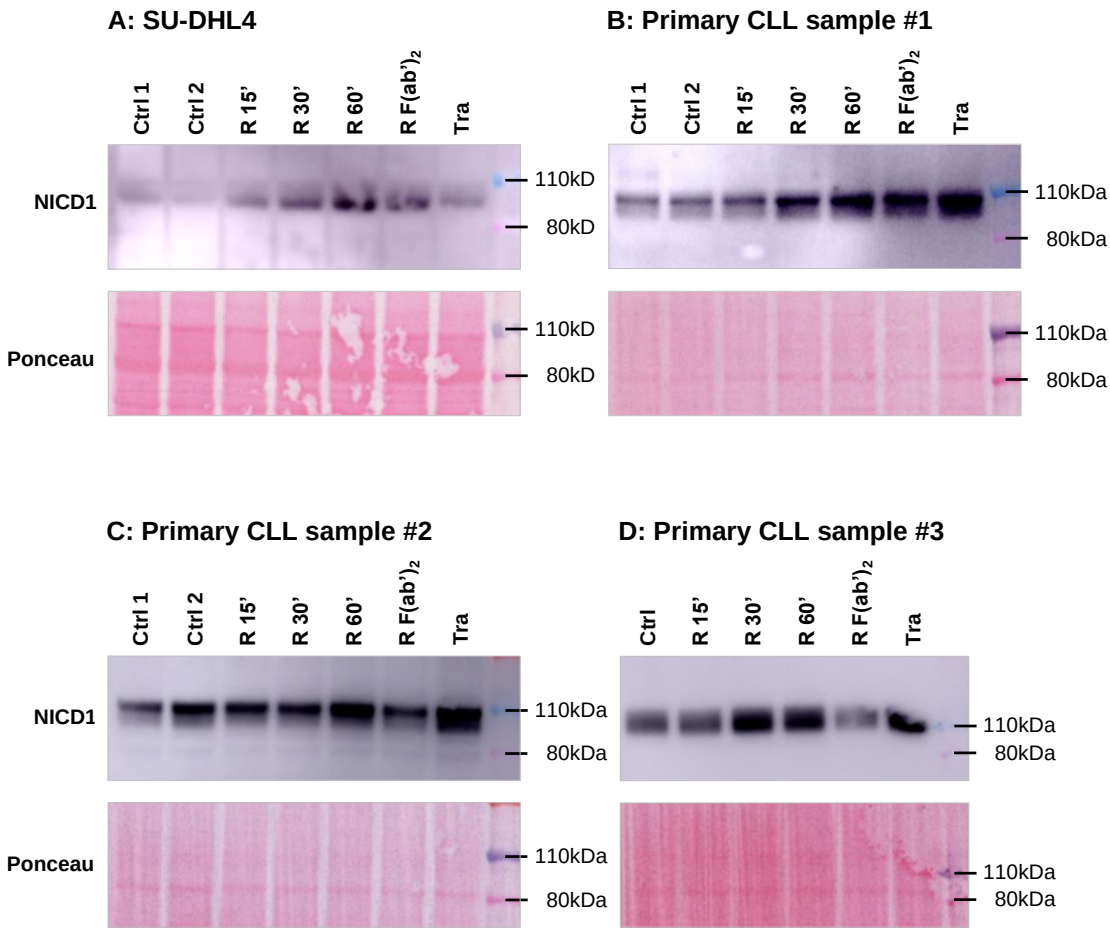

Supplementary Figure S7:

In primary CLL cells rituximab can increase NOTCH1 signaling via its F(ab‘)2 fragments and via its Fc-fragment.

Related to Figure 6.

Immunoblot detection of the NOTCH1 intracellular domain (NICD1) in SU-DHL4 cells (**A**) and in three primary CLL samples (**B-D**) treated with rituximab (R) for 15, 30 and 60 minutes, rituximab F(ab‘)$_2$ fragments (R F(ab‘)$_2$) for 60 minutes, or trastuzumab (Tra) for 60 minutes relative to untreated control samples (Ctrl).

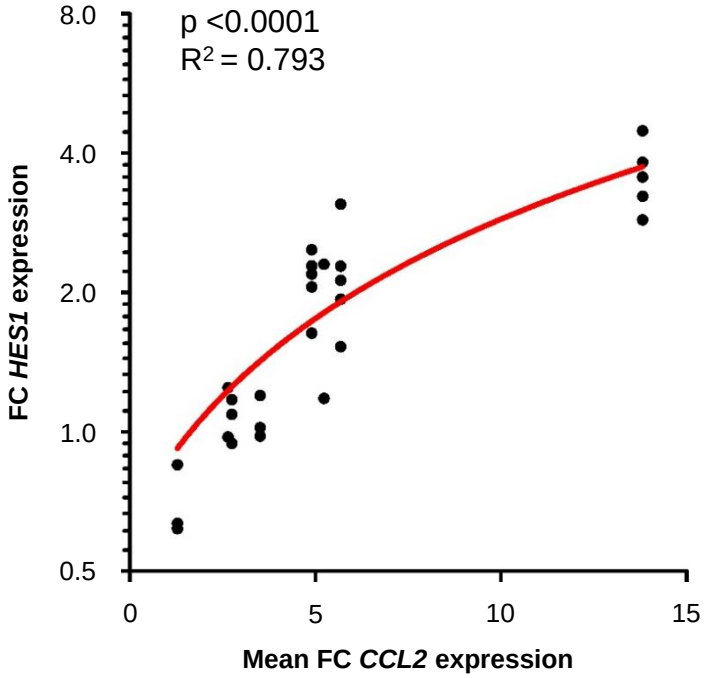

Supplementary Figure S8:

The increase in *HES1* expression after rituximab treatment correlated with the mean fold change of *CCL2* expression, used as surrogate marker for monocyte activation.

Related to Figure 6.

HES1 and *CCL2* expression was assessed in 8 individual CLL samples by qRT-PCR after 150 min of treatment with rituximab relative to untreated controls. Two to five biological replicates were used for each sample and treatment condition. The fold change (FC) of *HES1* expression was plotted against the mean FC of *CCL2* expression. Linear regression analysis was used to test for an association between the increase in *HES1* and *CCL2* expression.

Transparent Methods

Cells lines and patient samples

The B-cell lines SU-DHL4 derived from a germinal center B-cell type DLBCL (Epstein and Kaplan, 1979) and MEC1 derived from CLL in prolymphocytoid transformation (Stacchini et al., 1999) were obtained from American Type Culture Collection (ATCC, Manassas, VA, USA).

Peripheral blood samples were obtained from CLL patients attending St. Bartholomew's Hospital (Barts) and consenting to use of specimens for research. Peripheral blood mononuclear cells (PBMCs) were isolated via density gradient centrifugation (Lymphoprep®, Stemcell Technologies®, Vancouver, Canada) and enriched for B-cells via immunomagnetic beads against CD19 (MACS®, Miltenyi Biotec®, Bergisch Gladbach, Germany). To prevent activation of the NOTCH1 receptor during the isolation procedure, contact of cells with EDTA was avoided by the use of heparin monovettes and preparation of EDTA-free MACS sorting buffer. After sorting, CLL cells were used for downstream experiments immediately. White blood cell counts for the CLL samples used for Western blot analysis are provided below (as measured on the day of sample acquisition):

# CLL1	WBC: 158.0 x 10^9/l
# CLL2	WBC: 409,4 x 10^9/l
# CLL3	WBC: 73.8 x 10^9/l

Reagents

Cells were treated with the two anti-CD20 monoclonal antibodies rituximab and obinutuzumab. Trastuzumab was used as an isotype control. $F(ab')_2$ fragments were used to

study Fc-independent effects resulting exclusively from CD20 binding. The IgG B-cell receptor of SU-DHL4 was cross-linked by SB2H2.

Rituximab, trastuzumab and obinutuzumab were obtained from the local pharmacy of St. Bartholomew's hospital, London, United Kingdom. SB2H2 and rituximab F(ab')$_2$ fragments were in-house productions at the Centre of Cancer Immunology at Southampton University, Prof. Mark Cragg, and received as gifts. Hybridoma cell lines secreting the respective monoclonal antibodies were cultured and secreted antibodies were purified from the culture supernatant using protein A columns (GE Healthcare, Chicago, IL, USA). Purity of in-house monoclonal antibodies was assessed by electrophoresis (Beckman EP system, Beckman Coulter, Pasadena, CA, USA). Rituximab F(ab')$_2$ fragments were produced by standard pepsin digestions. The kinase inhibitors R406, ibrutinib and idelalisib were purchased from Selleckchem® at a concentration of 10mM/1ml in DMSO (Houston, TX, USA).

Cell culture

The SU-DHL4 cell line was maintained in Roswell Park Memorial Institute (RPMI) 1640 medium (Sigma-Aldrich®); the MEC1 cell line in Dulbecco's Modified Eagle Medium (DMEM; Sigma-Aldrich®). Medium was supplemented with 10% fetal bovine serum (FBS; Life Technologies®, Carlsbad, CA, USA) and 1% Penicillin/Streptomycin (Sigma-Aldrich®). Both cell lines were maintained at a concentration of 0.7 x 10^6 cells/ml at 37 °C and 5% CO2.

Monoclonal antibody treatment of SU-DHL4 cells and primary CLL cells

To assess signaling changes in the B-cell receptor cascade after monoclonal antibody treatment (*CCL4* and *CCL3* expression; phosphorylation of SYK, AKT and PRAS40) cells were re-suspended in their cell culture medium at a concentration of 1 x 10^6 cells/ml and treated with

the respective antibody at a concentration of 5 μg/ml for 1 h, 2.5 h or 24 h. Whole cell lysates for protein analysis were obtained after 1 h or 24 h. RNA was isolated after 2.5 h.

To assess short-term changes in NOTCH1 signaling after monoclonal antibody treatment (*HES1* alongside *CCL4* expression), SU-DHL4 cells were re-suspended in PBS at a concentration of 5 x 10^6 cells/ml. Immediately after re-suspension, cells were treated with the respective monoclonal antibody at a concentration of 2.5 μg/ml and kept in the incubator at 37 °C and 5% CO2 for 1 h. After 1 h, two volumes of RPMI were added to one volume of PBS and cells were kept in the incubator for another 1.5 hours before RNA isolation.

To assess long-term changes in NOTCH1 signaling, SU-DHL4 and MEC1 cells were used directly from the culture medium supplemented with inhibitors or vehicle control for 48 h (see below). Nuclear cell lysates were used for NICD1 immunoblots.

Treatment of SU-DHL4 and MEC1 cells with kinase inhibitors

The kinases Syk, Btk and Pi3K were inhibited by R406, ibrutinib and idelalisib, respectively. Cells were exposed to the inhibitors for 48 hours before subsequent experiments were conducted. Inhibitors were used at the following concentrations:

R406 and idelalisib	5 μM
Ibrutinib	1 μM

DMSO vehicle controls were kept alongside. PBS and culture medium added during the course of an experiment were supplemented with the respective inhibitor at concentrations mentioned above or with vehicle control.

Cell viability in each inhibitor and control condition was >90% after 48 hours.

Protein immunoblotting

For SYK, AKT and PRAS40 immunoblotting from whole cell lysates, cells were lysed with the Qproteome Mammalian Protein Prep Kit (Qiagen®, Hilden, Germany) according to the manufacturer's protocol. For NICD1 immunoblotting from nuclear protein fractions, cells were processed with NE-PER Nuclear and Cytoplasmic Extraction Reagents (Thermo Scientific, Waltham, MA, USA). Protein concentrations were determined by averaging three to four technical replicates measured on the NanoDrop® ND-1000 by using the Bradford dye-binding method (Protein Assay Dye Reagent Concentrate; Bio-Rad Laboratories, Hercules, CA, USA).

Lysates were separated by NuPAGE 4-12% Bis-Tris gels (Thermo Fisher Scientific) and transferred to PVDF membranes (Immobilon®, 0.45 µm pore size; Burlington, MA, USA) by wet electroblotting (17 hours, 30 Volts). Membranes were blocked with TBS with 1% skim milk powder (Sigma; St. Louis, MO, USA) and incubated with primary antibody for 1 hour at room temperature (see list of antibodies below). Following incubation, each membrane was washed four times with TBS supplemented with 0.1% Tween® 20 (Sigma-Aldrich, St. Louis, MO, USA), before incubation with a secondary horseradish peroxidase conjugated goat anti-rabbit antibody (GE Healthcare). Protein bands were visualized by using ECL Prime Western Blotting Detection Reagent (GE Healthcare) and the Amersham 600 imager (GE Healthcare).

The following primary antibodies were used for western blot analysis:

Cleaved NOTCH1 (Val1744)(D3B8) Rabbit mAb	Cell Signaling Technology®
Syk (D3Z1E) XP® Rabbit mAb	Cell Signaling Technology®
Phospho-Zap-70 (Tyr319)/Syk (Tyr352) (65E4) Rabbit mAb	Cell Signaling Technology®
Phospho-Syk (Tyr525/526) (C87C1) Rabbit mAb	Cell Signaling Technology®
Akt (pan) (C67E7) Rabbit mAb	Cell Signaling Technology®
Phospho-Akt (Ser473) (D9E) XP® Rabbit mAb	Cell Signaling Technology®
Phospho-Akt (Thr308) (D25E6) XP® Rabbit mAb	Cell Signaling Technology®

PRAS40 (D23C7) XP® Rabbit mAb	Cell Signaling Technology®
Phospho-PRAS40 (Thr246) (C77D7) Rabbit mAb	Cell Signaling Technology®
GAPDH (D16H11) XP® Rabbit mAb	Cell Signaling Technology®
Anti-Lamin B1 antibody (ab16048) Rabbit polyclonal antibody	Abcam®

Quantitative real-time polymerase chain reaction (qRT-PCR)

RNA was isolated by using the RNeasy Mini Kit (Qiagen®). Complementary DNA (cDNA) was generated from RNA using High-Capacity RNA-to-cDNA Kit® [Thermo Fisher Scientific®, Waltham, MA, USA] and 100 ng cDNA was subsequently used in 20 µl qRT-PCR reactions with TaqMan® Gene Expression Assays [Applied Biosystems®, Foster City, CA, USA]. *ACTB* or *18S* was used as endogenous control in 1:10 dilutions from the cDNA sample used for target gene analysis. Reactions were performed in triplicates on a QuantStudio™ 7 Flex System [Applied Biosystems®] using the standard thermal cycler protocol.

The following TaqMan® Gene Expression Assays were used:

HES1: Hs00172878_m1

CCL4: Hs01092201_m1

CCL3: Hs00234142_m1

CCL2: Hs00234140_m1

Fold changes were calculated towards the mean ΔCt-value of all reference samples.

Liquid chromatography tandem-mass spectrometry (LC-MS/MS) based phosphoproteomics

Briefly, cells were treated with rituximab or obinutuzumab (5 µg/ml) for 0h, 1h or 24 h in biological triplicates. Cells were lysed, protein concentrations normalized, proteins reduced and alkylated prior to tryptic digest. Subsequently, digests were desalted and underwent TiO2

based phospho-enrichment. Reconstituted samples were analyzed twice using an automated data-dependent acquisition on a Q-Exactive Plus mass spectrometer (Thermo Scientific). Peptide identification was conducted using Mascot Distiller 2.3.2 / Mascot Daemon 2.5 and label-free peptide quantification using in-house developed Peak statistics calculator (PESCAL) software. Extracted ion chromatograms were generated for each phosphopeptide ion and quantification values calculated by measuring areas under the curve. Analytical replicated (N=2) were averaged for each biological replicate (N=3). Quantified peptide ions that possessed the same phosphorylation site were combined. Differences in phosphorylation levels between each treatment group and the untreated control group were tested for significance by unpaired non-parametric t-tests conducted in GraphPad Prism version 8.1.1. Kinase activity was inferred by kinase substrate enrichment analysis (KSEA) as previously described (Casado et al., 2013). Pathway enrichment analysis was conducted through the Database for Annotation, Visualization and Integrated Discovery (DAVID) v6.8 (Huang da et al., 2009a; Huang da et al., 2009b). LC-MS/MS raw data is publicly available (PRIDE ID PXD023572).

A more detailed description of sample preparation, LC-MS/MS analysis and data processing is provided below.

Mass spectrometry sample preparation

1 x 10^7 SU-DHL-4 cells were either treated with rituximab or obinutuzumab for 1 or 24 hours, using a monoclonal antibody concentration of 5 μg/ml. Untreated controls were run in parallel. All conditions were run in biological triplicates.

Post antibody treatment, cell lysis, protein normalization, digestion, and phosphopeptide-enrichment were performed as previously described[43]. Briefly, cells were washed three times in cold PBS supplemented with 1 mM Na_3VO_4 and 1 mM NaF. Cells were then lysed in urea buffer (8 M urea in 20 mM HEPES pH 8.0 supplemented with 1 mM

Na_3VO_4, 1 mM NaF, 1 mM $Na_4P_2O_7$ and 1 mM sodium β-glycerophosphate). Cell extracts were sonicated (10 cycles of 30 sec on and 40 sec off; Bioruptor® Plus, Diagenode, Liege, Belgium). Insoluble material was removed by centrifugation at 15,000 rpm for 10 min at 4 ˚C.

Protein was quantified by bicinchoninic acid (BCA) assay (Pierce™ BCA Protein Assay Kit, Thermo Fisher Scientific), and 350 µg of protein was reduced and alkylated by sequential incubation with 10 mM DTT and 16.6 mM iodoacetamyde for 40 minutes. Urea concentration was diluted to 1.44 M with 20 mM HEPES (pH 8.0), prior to the addition of preconditioned trypsin beads as per manufacturers specifications [(Immobilized Trypsin, TPCK Treated, Thermo Fisher Scientific)] and incubation for 18h at 37 ˚C. Trypsin beads were removed by centrifugation at 2,000 x g for 5 min at 4˚C.

Peptide solutions were desalted using 10 mg OASIS-HLB cartridges (Waters, Manchester, UK). Cartridges were activated with ACN (100%) and equilibrated with 1.5 mL washing solution (1% ACN, 0.1% TFA). After loading the samples, cartridges were washed with 1 mL of washing solution. Peptides were eluted with 500 µL of glycolic acid buffer (1 M glycolic acid, 50% ACN, 5% TFA).

To enrich phosphopeptides, sample volumes were normalised to 600 µL using glycolic acid buffer (1 M glycolic acid, 80% ACN, 5% TFA) and 50 µL of TiO_2 beads [(50% slurry in 1% TFA), GL Sciences, Shinjuku, Tokio, Japan] were added to the peptide mixture and incubated for 5 min at room temperature with agitation and centrifuged for 30 s at 1,500 x g. Pelleted TiO_2 beads were then loaded into an empty PE-filtered spin-tip (Glygen, Columbia, MD, USA) prewashed with ACN and packed by centrifugation at 1500 x g for 3 min. The remaining supernatants were then applied to respective spin tips by centrifugation at 1,500 x g for 2 min, and then sequentially washed by 3 min centrifugation at 1,500 x g with glycolic acid buffer, 100 mM ammonium acetate (25% ACN) and 10% ACN. For phosphopeptide recovery,

peptides were eluted with 5% ammonium water. Eluents were dried in a speed vac and peptide pellets stored at -80 ˚C.

LC-MS/MS analysis

For LC-MS/MS analysis, peptides were resuspended in 12 µL of reconstitution buffer (97% H20, 3% ACN, 0.1% TFA, 50 fmol/µl-1 enolase peptide digest), sonicated for 1 min at room temperature and placed in the autosampler (4 °C) until analyzed. Each sample was analyzed twice (4 µl injections). The LC-MS/MS system consisted of a nanoflow ultrahigh pressure liquid chromatography system (UltiMate^{TM} 3000 RSLCnano, Dionex, Sunnyvale, CA, USA) coupled to a Q-Exactive Plus (Thermo Fisher Scientific).

The LC system used mobile phases A (3% ACN: 0.1% FA) and B (100% ACN; 0.1% FA). Peptides were loaded onto a µ-pre-column (Thermo Fisher Scientific) and separated in an analytical column (EASY-Spray, Thermo Fisher Scientific). The gradient was 1% B for 5 min, 1% B to 35% B over 60 min. Following elution, the column was washed with 85% B for 7 min and equilibrated with 3% B for 7 min at a flow rate of 0.25 µL/min. Peptides were nebulized into the online connected Q-Exactive Plus system operating with a 2.1s duty cycle. Acquisition of full scan survey spectra (m/z 375-1,500) with a 70,000 FWHM resolution was followed by data-dependent acquisition in which the 15 most intense ions were selected for HCD (higher energy collisional dissociation) and MS/MS scanning (200-2,000 m/z) with a resolution of 17,500 FWHM. A 30 sec dynamic exclusion period was enabled with an exclusion list with 10 ppm mass window. Overall duty cycle generated chromatographic peaks of approximately 30 sec at the base, which allowed the construction of extracted ion chromatograms (XICs) with at least 10 data points.

Peptide identification and quantification

Mascot Distiller 2.3.2 was used to fit an ideal isotopic distribution to the MS/MS data to maximize peptide identification. Mascot Daemon 2.5 search engine was used to match peaks to peptides in proteins present in the Uniprot/SwissProt Database (human species). The process was automated with Mascot Daemon 2.5.0. Mass tolerance was set to ± 10 ppm, with variable modifications phospho (ST), phospho (Y), gln→pyro-glu (N-term Q) and oxidation (M) included in the search. Carbamidomethyl (C) as fixed modification. Trypsin was selected as digestion enzyme and 2 miss cleavages were allowed. Sites of modification were reported when they had delta scores >10.

Peptide and subsequent protein quantification was achieved using in-house developed PESCAL (Peak statistics calculator) software (Cutillas, 2017). PESCAL constructs extracted ion chromatograms (XICs) for each peptide identified with the MASCOT search engine. With each constructed XIC, peak heights could be calculated. These peptide peak heights were then normalized to the sum of the intensities for each individual sample and the average fold change between conditions could be determined. Statistical significance between conditions was considered significant when the Student T-Tests produced $P < 0.05$. Further data processing and analysis was conducted within Microsoft Excel (2007/2010) or R (v3.3.2/v3.4.1 – reshape2, ggplot2, gplots, readXL, Hmisc and limma packages).

Kinase substrate enrichment analysis (KSEA) was performed as described before (Casado et al., 2013). Briefly, peptides differentially phosphorylated between a set of samples were grouped into substrate sets known to be phosphorylated by a specific kinase as annotated in the PhosphoSite, Phospho.ELM, and PhosphoPOINT databases (Hornbeck et al., 2015; Dinkel et al., 2011; Yang et al., 2008). To infer enrichment of substrate groups across sets of samples the hypergeometric test was used, followed by Benjamini Hochberg multiple testing correction.

Supplemental references

Casado, P., Rodriguez-Prados, J. C., Cosulich, S. C., Guichard, S., Vanhaesebroeck, B., Joel, S. & Cutillas, P. R. (2013). Kinase-substrate enrichment analysis provides insights into the heterogeneity of signaling pathway activation in leukemia cells. Sci Signal 6**,** rs6.

Cutillas, P. R. (2017). Targeted In-Depth Quantification of Signaling Using Label-Free Mass Spectrometry. Methods Enzymol 585**,** 245-268.

Dinkel, H., Chica, C., Via, A., Gould, C. M., Jensen, L. J., Gibson, T. J. & Diella, F. (2011). Phospho.ELM: a database of phosphorylation sites--update 2011. Nucleic Acids Res 39**,** D261-267.

Epstein, A. L. & Kaplan, H. S. (1979). Feeder layer and nutritional requirements for the establishment and cloning of human malignant lymphoma cell lines. Cancer Res 39**,** 1748-1759.

Hornbeck, P. V., Zhang, B., Murray, B., Kornhauser, J. M., Latham, V. & Skrzypek, E. (2015). PhosphoSitePlus, 2014: mutations, PTMs and recalibrations. Nucleic Acids Res 43**,** D512-520.

Huang Da, W., Sherman, B. T. & Lempicki, R. A. (2009a). Bioinformatics enrichment tools: paths toward the comprehensive functional analysis of large gene lists. Nucleic Acids Res 37**,** 1-13.

Huang Da, W., Sherman, B. T. & Lempicki, R. A. (2009b). Systematic and integrative analysis of large gene lists using DAVID bioinformatics resources. Nat Protoc 4**,** 44-57.

Stacchini, A., Aragno, M., Vallario, A., Alfarano, A., Circosta, P., Gottardi, D., Faldella, A., Rege-Cambrin, G., Thunberg, U., Nilsson, K. et al. (1999). MEC1 and MEC2: two new cell lines derived from B-chronic lymphocytic leukaemia in prolymphocytoid transformation. Leuk Res 23**,** 127-136.

Yang, C. Y., Chang, C. H., Yu, Y. L., Lin, T. C., Lee, S. A., Yen, C. C., Yang, J. M., Lai, J. M., Hong, Y. R., Tseng, T. L., et al. (2008). PhosphoPOINT: a comprehensive human kinase interactome and phospho-protein database. Bioinformatics 24**,** i14-20.